Nuclear level mixing-induced interference in $FeCO_3$

2008 J. Phys.: Condens. Matter 20 485214

(http://iopscience.iop.org/0953-8984/20/48/485214)

IOP PUBLISHING JOURNAL OF PHYSICS: CONDENSED MATTER

J. Phys.: Condens. Matter **20** (2008) 485214 (12pp) doi:10.1088/0953-8984/20/48/485214

Nuclear level mixing-induced interference in $FeCO_3$

S Gheysen and J Odeurs

Instituut voor Kern- en Stralingsfysica, Katholieke Universiteit Leuven, Celestijnenlaan 200D, B-3001 Leuven, Belgium

E-mail: jos.odeurs@fys.kuleuven.be

Received 2 January 2008, in final form 12 September 2008
Published 28 October 2008
Online at stacks.iop.org/JPhysCM/20/485214

Abstract

We present a detailed description and a consistent explanation of the transparency observed in the Mössbauer absorption spectra at a nuclear level mixing in $FeCO_3$. We develop a model for scattering in this nuclear Λ system in a Maxwell–Schrödinger approach, taking into account multiple scattering and polarization effects. It is shown that the level mixing scheme not only yields an expected Stark splitting, but, due to the unequal relaxation rates and transition strengths, an additional interference term is present. Therefore, this scheme is equivalent to the Λ scheme considered for EIT in quantum optics. The interference in the absorption of the gamma radiation can be destructive, leading to a partial transparency, but can also be constructive. Both types of interference are present in the observed spectra.

1. Introduction

Five years ago, a partial reduction of absorption was observed at a nuclear level crossing in a single $FeCO_3$ crystal [1]. This transparency was quickly designated as the first observation of electromagnetically induced transparency (EIT) [2] for *gamma* radiation. Thereafter it was recognized, however, that the nuclear level mixing scheme is not identical to a typical three-level Λ scheme in quantum optics [3]. In the latter scheme the two lower lying states are (meta)stable, which is a necessary condition to induce interference. It is readily shown that, if the coupling levels have exactly equal decay rates, all interference vanishes. In this case, however, it is not possible to fully explain the experimental data. More specifically, the lack of an appreciable reduced absorption in a second Λ scheme in the perpendicular geometry, where the radiation is incident perpendicular to the symmetry axis, poses a hard challenge for our models.

This paper now aims to provide a fully consistent explanation of the transparency observed in *both* experimental geometries. The key lies in the presence of an additional relaxation mechanism, which yields different relaxation rates for the levels involved in the different Λ schemes.

Previous theoretical studies [4] have already shown that this nuclear level mixing scheme yields the creation and enhancement of radiation with a polarization complementary to the incident radiation. This radiation contributes to the reduction of absorption and is delayed with respect to the incident radiation.

We want to emphasize that these dynamical and polarization-dependent effects are also incorporated in the model discussed here. Moreover, this is the first time that we present *quantitative* fits of the experimental results in both geometries.

In section 2 the set-up and results of the Mössbauer experiments are described. We first discuss the relevant properties of the $FeCO_3$ crystal including the effects of the impurities. After briefly reviewing some features of Mössbauer spectroscopy, the spectra are presented along with a crude analysis using Lorentzian absorption lines.

In section 3 a theoretical model for nuclear scattering in a three-level scheme is developed based on the semiclassical Maxwell–Schrödinger approach. The results for both equal and unequal relaxation rates of the coherences involving the excited levels are first analyzed analytically in the thin absorber limit. The full expressions are then solved numerically in order to find a best fit of the experimental spectra.

Conclusions are drawn in section 4.

2. $FeCO_3$ Mössbauer experiments

2.1. $FeCO_3$ single crystal

Ferrous carbonate or $FeCO_3$, naturally occurring as the mineral *siderite*, chemically belongs to the carbonate group

and structurally to the calcite ($CaCO_3$) subgroup (hexagonal space group $R\bar{3}c$). The threefold symmetry of the triangular carbonate groups explains the trigonal symmetry of the $FeCO_3$ crystal. In a pure single crystal the principal axis of the axially symmetrical electric field gradient (efg) then coincides with this symmetry axis, which will be referred to as the c axis.

Natural siderite, however, is usually impure, with impurities quoted up to 17% [5–11], mainly Mg and Mn, possibly Ca and Zn. All of them are chemically equivalent to Fe. Because the Mg and Mn ions have similar ionic radii (0.072 and 0.083 nm, respectively, compared with 0.078 nm of the Fe ion [12]), they are expected to be found on substitutional sites. Complete series of $Fe_xMg_{1-x}CO_3$ and $Fe_xMn_{1-x}CO_3$ are possible [13]. A Ca ion has an appreciably larger radius (0.100 nm [12]) and will not so easily substitute for Fe. It is well documented, however, that calcite can appear as a coexisting carbonate species in the siderite crystal structure [13].

The chemical composition of our siderite crystal has been obtained through an atomic absorption spectroscopy study. Expressed in atomic proportions, the total cation content of the sample is 84.2% Fe, 8.1% Ca and 6.4% Mn with small traces (<1%) of Na, Al, Mg, K and Sr.

The 6.4% Mn content on substitutional lattice sites can disturb the axial efg at the Fe site. *Ab initio* calculations [14] show that an Mn impurity can have a small, but non-negligible, influence on the efg. If one of the six nearest neighbors of Fe is replaced by Mn, the axial symmetry is broken. Such a small non-axial symmetrical component of the efg can play the role of a mixing field between two crossing nuclear levels, as will be clear later on.

It is known that $FeCO_3$ is paramagnetic at high temperatures, but it becomes antiferromagnetic below the Néel temperature of $T_N \approx 38$ K [6, 9–11], with the magnetic field collinear with the axis of the efg. At low temperatures, spins of the neighboring Fe ions order in an antiparallel way while the next-nearest neighbors order in a parallel way. Furthermore, the magnetic hyperfine field displays a particular temperature dependence. The magnetic field increases with decreasing temperature and saturates at $T \approx 18$ K to a value of $B \approx 18$ T [7, 9, 10]. This is explained by fluctuations between the two low-lying electronic states, which respectively yield $+B$ and $-B$ [10].

Below T_N the hyperfine structure of the ^{57}Fe nucleus in a pure $FeCO_3$ single crystal is fully described by a quadrupole splitting due to the efg and a temperature-dependent Zeeman splitting due to the magnetic field. In the case of the axial symmetry, the resulting hyperfine levels of the $I_g = 1/2$ ground and $I_e = 3/2$ excited states are pure magnetic quantum number states, labeled by $m_g = \pm 1/2$ and $m'_e = \pm 1/2,\ \pm 3/2$, respectively, see figure 1.

It is seen that, at the temperature of $T \approx 31$ K, the $|m_e = 1/2\rangle$ and $|m'_e = -3/2\rangle$ levels accidentally cross. These crossing levels are very sensitive to the presence of a non-axial component of the efg, which could be induced by impurities. It has already been argued before [3] that a non-axial efg component perturbs the crossing $\Delta m = |m_e - m'_e| = 2$ levels in first order. Hence, this small perturbation can act as a mixing interaction and can yield observable effects at the level crossing, without disturbing the other hyperfine levels.

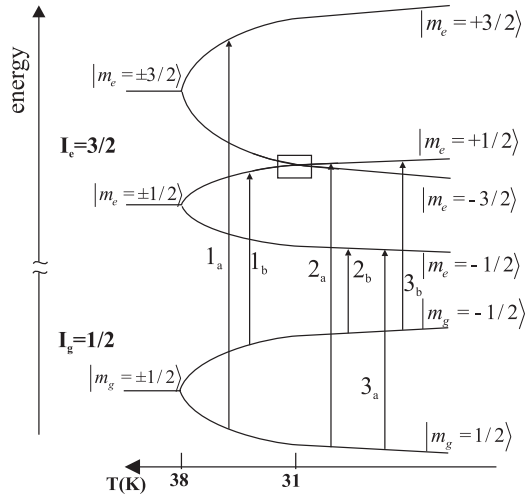

Figure 1. The hyperfine level structure of the $I_g = 1/2$ ground and $I_e = 3/2$ excited state of the ^{57}Fe nucleus in $FeCO_3$ as a function of temperature. The rectangle shows the $|m_e = -3/2\rangle$–$|m_e = 1/2\rangle$ level crossing at $T = 31$ K. The six allowed transitions are grouped into three doublets, see the text.

2.2. *Mössbauer experiment*

Mössbauer spectroscopy is a very successful technique applied by a worldwide and interdisciplinary group of researchers who are interested in harvesting environmental information at the nuclear level. At the heart of the technique lies the so-called Mössbauer effect, named after its discoverer Mössbauer [15]. The Mössbauer effect is an elastic process of (gamma) photon emission and absorption without observable recoil of the nucleus/nuclei involved. The probability for a recoil-free emission and absorption is given by the Debye–Waller [16] or Lamb–Mössbauer factor [17] f.

There has been some controversy in deducing the Lamb–Mössbauer factor in $FeCO_3$. Goldanskii *et al* [18] first reported a highly anisotropic f, which was explained as the Goldanskii–Karyagin effect. This was later refuted by the work of Housley *et al* [8, 19], which correctly included the polarization dependence of the absorption lines. The most recent values of the Lamb–Mössbauer factor in $FeCO_3$ are $f_{\mathbf{k}\parallel c} = 0.72(2)$ and $f_{\mathbf{k}\perp c} = 0.75(2)$ (at 300 K) [11], which confirm the lack of spatial anisotropy.

The conventional Mössbauer set-up includes a radioactive source (here ^{57}Co in a Rh matrix) that is mounted on a velocity transducer, which was in the constant acceleration mode, with velocities in the range [-7 mm s^{-1}, 7 mm s^{-1}]. The Doppler shift of the energy of the emitted gamma radiation in this range allows for a resonant scan of the hyperfine energy structure of the sample under investigation.

The sample is mounted on top of the cold finger, which is temperature-controlled by a helium flow cryostat. The temperature was stabilized to 0.1 K and calibrated at the boiling point of liquid nitrogen. In principle, the cold finger

allows operating temperatures down to 4.2 K. Finally, a Kr gas proportional counter detects the transmitted radiation.

The signal processing set-up also has a standard configuration. The linewidth of the source was close to the minimum linewidth, and the linewidth (HWHM) of the two inner lines of the calibration spectrum, with a thin non-enriched iron foil as absorber, was 0.125(1) mm s^{-1}.

As we are dealing with a *single* crystal with a preferential direction (crystal or c axis), we can define the direction of the incident source radiation **k** with respect to this axis. The angle (θ) between the incident radiation and the c axis can be varied by a rotation around the cold finger axis. Two geometries are studied, i.e. the 'parallel geometry' ($\theta = 0$) and the 'perpendicular geometry' ($\theta = \pi/2$). Note that because the angle (β) of the c axis to the crystal surface (cleavage plane) is ≈45°, the effective thickness of the crystal is the same in both geometries.

The $FeCO_3$ crystal has a physical thickness of $d = 168\ \mu$m. A dimensionless effective optical thickness can be defined as

$$T_e = \sigma_0 f \chi \rho \frac{d}{\sin(\beta + \theta)}, \tag{1}$$

with σ_0 the maximal resonant absorption cross section, f the recoil-free fraction, χ the isotopic enrichment or natural isotopic abundance of ^{57}Fe and ρ the concentration of Fe in the crystal. Because the radiation is incident at an angle $\pi - (\beta + \theta)$ with respect to the crystal surface, the distance traveled through the crystal is larger than for normal incidence. According to its definition, T_e can be interpreted as the number of resonant scattering events that take place during the propagation of the gamma radiation through the crystal. The value of T_e for the $d = 168\ \mu$m $FeCO_3$ crystal, taking into account the geometry of the set-up, the measured impurity percentages and the general parameters of ^{57}Fe, is calculated as $T_e = 7.9 \approx 8$.

2.3. First analysis

The presentation of the measured Mössbauer spectra in the next section already includes a first crude Lorentzian analysis. This analysis still assumes a perfect axially symmetrical crystal, i.e. without mixing interaction.

The data are fitted with the Recoil program [20], using the 'Lorentzian absorption profile' procedure. This fitting procedure simply tries to find a best fit $f(v)$ by fitting each absorption line i with a Lorentzian profile $L_i(v)$:

$$f(v) = \mathrm{BG} - \sum_i L_i(v) \tag{2}$$

with

$$L_i(v) = \frac{A_i}{\pi} \frac{\Gamma_i}{(v - v_i)^2 + \Gamma_i^2} \tag{3}$$

where BG is the spectral background, A_i is the area, v_i the resonance velocity and Γ_i the half-width of the absorption line.

The number of free parameters can be considerably reduced by taking into account two physics 'rules'. First, according to parity invariance, the (m_e, m_g) and $(-m_e, -m_g)$ transitions are equal in all of their properties. Here, this means that they have the same A and Γ. Second, as is well known, the positions of the absorption lines v_i are related through the underlying hyperfine interaction physics, i.e. the quadrupole and Zeeman splitting.

Since the electromagnetic interaction of the ^{57}Fe nucleus with gamma radiation has mainly a magnetic dipole (M1) character, the interaction Hamiltonian $\mathcal{H}^\sigma$, for a particular polarization σ, can be written as [21]

$$\mathcal{H}^\sigma_{\mathrm{M1}} = \sum_{\Delta m=-1}^{1} D^1_{\Delta m,\sigma}(-\phi, -\theta, 0)\mathcal{H}(\Delta m), \tag{4}$$

where $\mathcal{H}(\Delta m)$ designates the electromagnetic interaction that induces a Δm transition. In this expression $(0, \theta, \phi)$ are the Euler angles that describe the orientation of the incident radiation (**k**) in the crystal axis system (e.g. the principal axis system of the efg). The $D^1_{\Delta m,\sigma}(-\phi, -\theta, 0)$ coefficients describe the Wigner matrix elements. Explicit expressions for interaction with $\sigma = \pm 1$ polarized radiation are given by

$$\mathcal{H}^+_{\mathrm{M1}} = \cos^2\frac{\theta}{2} e^{i\phi}\mathcal{H}^+(\Delta m = +1) + \frac{1}{\sqrt{2}}\sin\theta\mathcal{H}^+(\Delta m = 0) + \sin^2\frac{\theta}{2} e^{-i\phi}\mathcal{H}^+(\Delta m = -1) \tag{5}$$

$$\mathcal{H}^-_{\mathrm{M1}} = \sin^2\frac{\theta}{2} e^{i\phi}\mathcal{H}^-(\Delta m = +1) - \frac{1}{\sqrt{2}}\sin\theta\mathcal{H}^-(\Delta m = 0) + \cos^2\frac{\theta}{2} e^{-i\phi}\mathcal{H}^-(\Delta m = -1). \tag{6}$$

This means that in the parallel geometry ($\theta = 0$) each circular polarization can induce only one transition according to $\Delta m = \sigma$, whereas if $\theta \neq 0$ each polarization induces three Δm transitions. So, in general, there are six possible gamma transitions (m_e, m_g) between the $I_e = 3/2^-$ and $I_g = 1/2^-$ states. According to the parity invariance, these six lines can be grouped in three doublets. These doublets, their splittings Δv_i and center shifts CS_i are identified as (see also figure 1)

doublet 1: $(3/2, 1/2) - (-3/2, -1/2)$
with $\Delta v_1 = 3\beta_e + \beta_g$, $\mathrm{CS}_1 = \mathrm{IS} + \Delta/2$

doublet 2: $(1/2, 1/2) - (-1/2, -1/2)$
with $\Delta v_2 = \beta_e + \beta_g$, $\mathrm{CS}_2 = \mathrm{IS} - \Delta/2$

doublet 3: $(1/2, -1/2) - (-1/2, 1/2)$
with $\Delta v_3 = \beta_g - \beta_e$, $\mathrm{CS}_3 = \mathrm{IS} - \Delta/2$

where we have defined IS as the isomer shift[1]

$$\beta_g = \frac{c}{E_\gamma}\hbar\omega_{L,g}, \tag{7}$$

$$\beta_e = -\frac{c}{E_\gamma}\hbar\omega_{L,e}, \tag{8}$$

and

$$\Delta = \frac{c}{E_\gamma} 6\hbar\omega_Q, \tag{9}$$

with $\omega_{L,g/e}$ the Larmor frequency of the ground/excited state, ω_Q the quadrupole frequency, c the velocity of light in vacuum

[1] The isomer shift is the nuclear analogue of the chemical shift. It essentially measures the difference in the electrostatic interaction between a source and absorber nucleus with their respective environment [22].

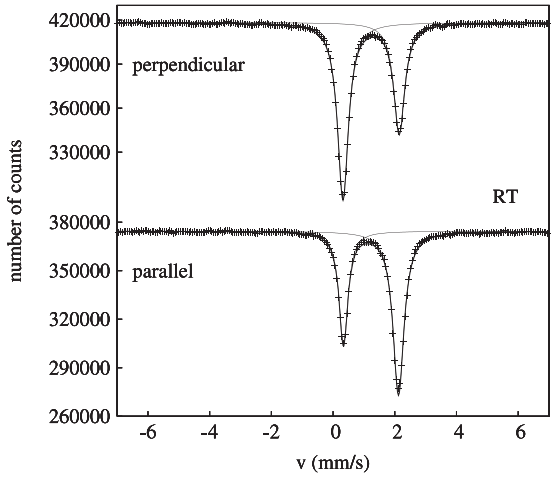

Figure 2. Mössbauer spectra at RT and for both perpendicular and parallel geometries. The solid line gives the best Lorentzian fit.

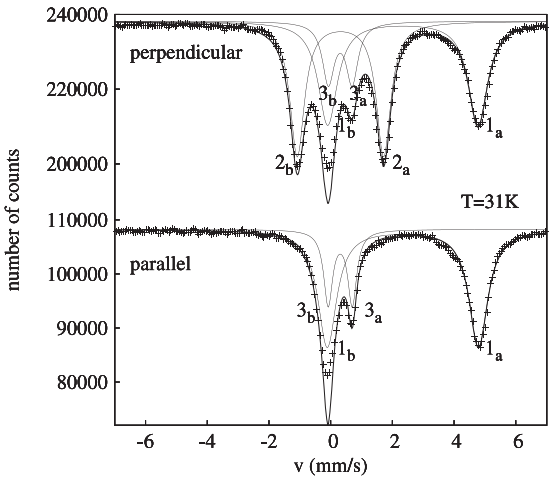

Figure 4. Mössbauer spectra at $T = 31$ K for both the perpendicular and parallel geometries. The solid line gives the best Lorentzian fit.

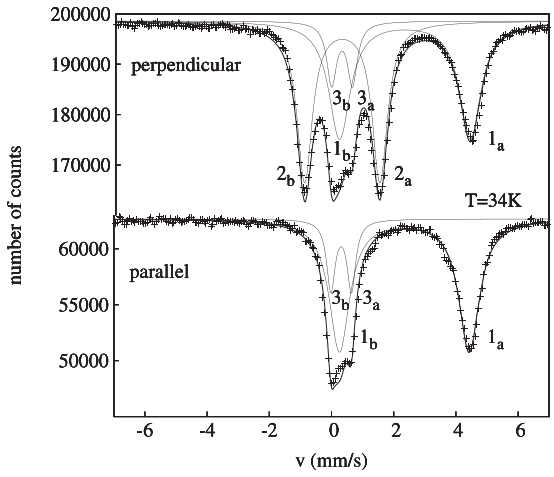

Figure 3. Mössbauer spectra at $T = 34$ K for both the perpendicular and parallel geometries. The solid line gives the best Lorentzian fit.

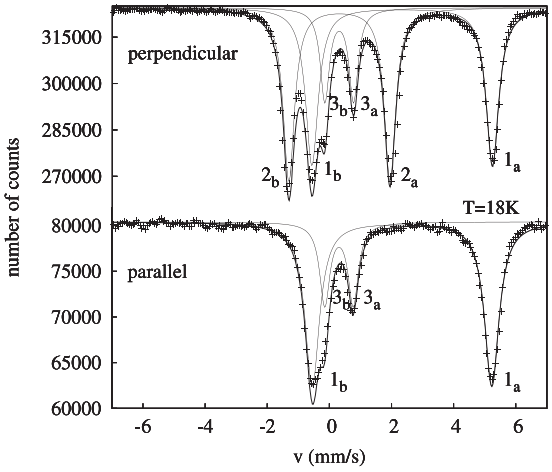

Figure 5. Mössbauer spectra at $T = 18$ K for both the perpendicular and parallel geometries. The solid line gives the best Lorentzian fit.

and $E_\gamma = 14.413$ keV the energy of the gamma radiation. Because β_e and β_g are related to each other, all Δv_i's are fixed as soon as one doublet is fitted.

In summary, taking into account the above arguments, the fitting function $f(v)$ is now the sum of three Lorentzian doublets:

$$f(v) = BG - \sum_{i=1}^{3} \frac{A_i}{2\pi} \left(\frac{\Gamma_i}{(v - (\mathrm{CS}_i - \Delta v_i))^2 + \Gamma_i^2} + \frac{\Gamma_i}{(v - (\mathrm{CS}_i + \Delta v_i))^2 + \Gamma_i^2} \right). \quad (10)$$

The application of 'basic' physics knowledge has reduced the number of fitting parameters[2] from 19 to 10: the background BG, the area A_i and half-width Γ_i of each doublet, the isomer shift IS, the quadrupole splitting Δ and the magnetic hyperfine splitting β_g (or β_e).

[2] This is in the case of a non-parallel geometry. In the parallel geometry the number of fitting parameters is reduced from 13 to 8.

2.4. Spectra

Although we have recorded Mössbauer spectra for many temperatures, we only highlight the spectra at room temperature (RT), see figure 2, and for three temperatures below T_N, i.e. for $T = 34$, 31 and 18 K in figures 3, 4 and 5, respectively.

At RT, the quadrupole splitting of the excited state, as shown in figure 1, is observable as a doublet in the absorption spectrum. The areas of the absorption lines are thickness- and polarization-dependent and therefore differ for the two geometries. This effect is well described in [19].

We are particularly interested in the spectra recorded for temperatures around the level crossing temperature. For $T < T_N$, the values of the parameters deduced from the fits are graphically presented in figure 6. This includes the fitting values from spectra at different temperatures that are not shown explicitly. The center shifts are not displayed because they were held fixed for all spectra at $\mathrm{CS}_1 = 2.34$ mm s^{-1} and $\mathrm{CS}_2 = \mathrm{CS}_3 = 0.31$ mm s^{-1}. In the perpendicular

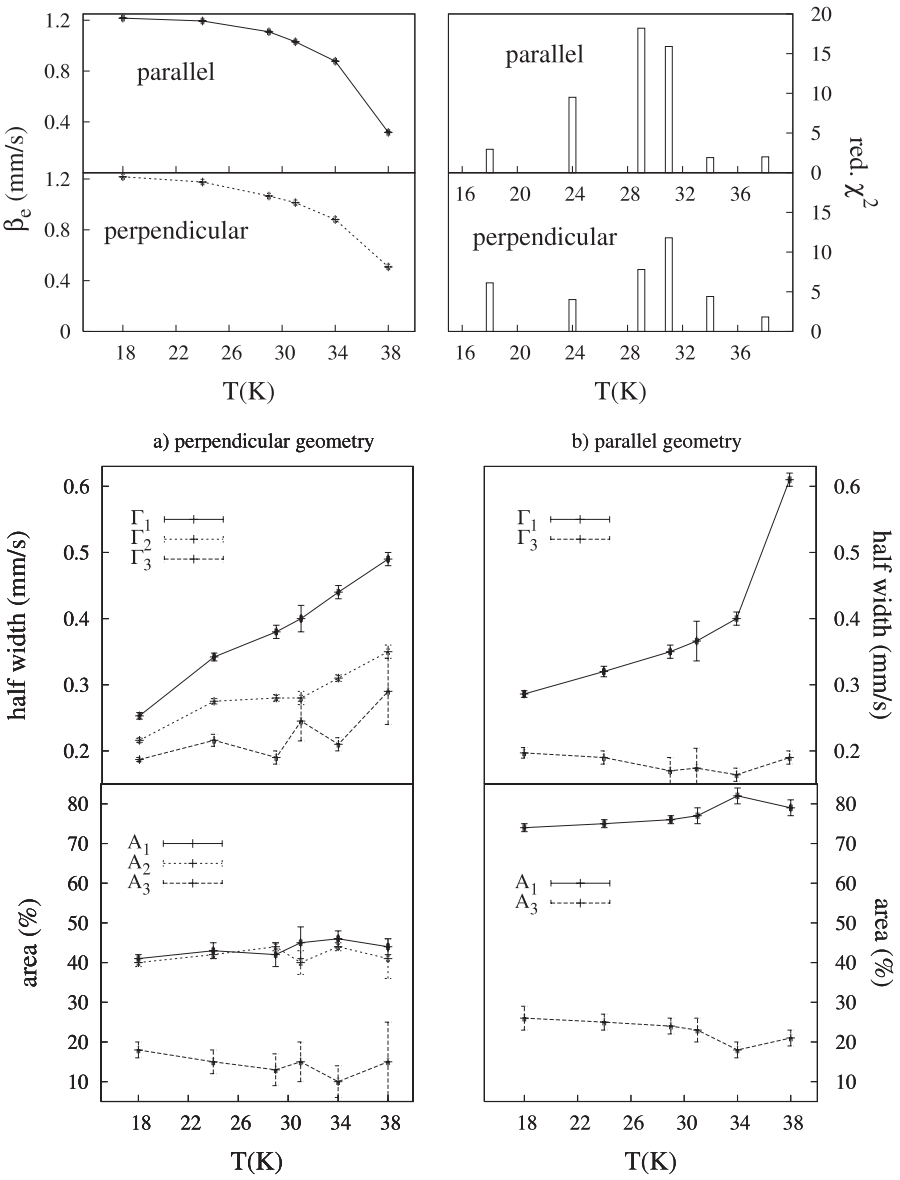

Figure 6. Graphical presentation of the fitting results of the Mössbauer spectra of $FeCO_3$, below T_N. The top left figure shows the temperature dependence of the Zeeman splitting of the two reference doublets. The top right figure gives the values of the reduced χ^2 of each fit. The deduced linewidths and areas of the Lorentzian doublets for both geometries are displayed in the bottom figures.

geometry, we first fit the splitting of the doublet 2 because its absorption lines are best resolved. Due to the absence of the second doublet in the parallel geometry, the splitting of the first doublet is taken as a reference. From the values for Δv_1 and Δv_3 a value for β_e for both geometries is calculated according to equation (8). They are shown in the upper left part of figure 6. In the same figure, the reduced χ^2 of each spectrum is given as a measure of the goodness-of-fit.

Clearly, for $T = 29/31$ K the discrepancy between experiment and the model is the largest. At the level crossing ($v \approx -0.16$ mm s^{-1}) the difference between the predicted Lorentzian fit and the experimental data amounts to 25% of the absorption line. There is less absorption observed than predicted by the fit. Therefore, we can say that the absorption line has become (partially) transparent.

A few other interesting remarks can be deduced from the spectra and their first analysis. First, in figure 6 the temperature dependence of β_e, which is proportional to the magnetic hyperfine field through $\omega_{L,e}$, displays a similar behavior for both geometries. This is in agreement with the temperature dependence reported in [10]. For decreasing temperatures, the magnetic hyperfine field reaches a saturation value. At 18 K, we deduce that $B^{\perp}_{18\,K} = 17.98(2)$ T and $B^{\parallel}_{18\,K} = 17.96(2)$ T, which fall within a 2σ interval of the $B_{\approx 18\,K} = 18.3(3)$ T value reported in [10].

Secondly, in figure 6 the widths of the three doublets vary widely, although they involve transitions to the same nuclear excited state, embedded in a particular chemical environment. In the parallel case, it is seen that the temperature behavior of the doublets is also quite different. An explanation of this phenomenon is given in terms of fluctuating hyperfine

fields [23, 24]. As the Larmor frequency of the doublets differs, they respond in a different way to a fluctuating magnetic field. Doublet 1 has the highest Larmor frequency and hence is most strongly influenced by a change in the magnetic field. It 'feels' a more blurred magnetic field, which causes a larger linewidth than for the other doublets. This corresponds to an additional relaxation rate, which is most pronounced in the case of the $|m_e = \pm 3/2\rangle$ levels. If this interpretation is correct, then the linewidths should decrease with decreasing temperature, which is clearly seen in figure 6. Extrapolation shows that the linewidth (HWHM) of doublet 1 at 10 K is about 0.17 mm s^{-1} which, when taking into account the experimental line broadening, is consistent with the calculated width corresponding to a thickness characterized by $T_e \approx 9$.

Thirdly, the areas of the doublets remain more or less constant in this low-temperature interval. Because the area of a Mössbauer absorption line depends on the effective thickness T_e, the angle of incidence θ and the magnetic quantum numbers of the levels involved (see, e.g., [8]), it is expected that this value is indeed temperature-independent.

Before embarking on our in-depth study of the reduction of absorption at the level crossing, it is necessary to refute the hypothesis of saturation as a sufficient explanation. We must, however, make a distinction between the two geometries. In the perpendicular geometry, each polarization state of the incident radiation can induce all three Δm transitions. Hence, at the level crossing, the interaction strength of each polarization state has doubled with respect to a non-crossing situation. This can be seen as radiative interaction with an absorber that has doubled its thickness. However, due to saturation, a doubling of the thickness does not automatically yield a doubling of the absorption. There is always less absorption, but how much less depends on the initial thickness of the absorber. It can be shown that for $T_e = 8$ the effect of saturation is already important. Moreover, the reduced absorption in the perpendicular geometry can even be quantitatively explained in a model that includes thickness effects.

Things are quite different in the parallel geometry. Now gamma radiation with a polarization state that can induce one of the transitions involved in the level crossing cannot induce the other one, even if the levels cross. It is clear that in this case no doubling of the interaction strength occurs. Therefore, the hypothesis of saturation as solely responsible for the reduced absorption is not tenable.

In order to fully understand these experimental results we develop a model for nuclear resonant scattering that incorporates not only the necessary thickness and polarization dependence, but also takes into account an interaction that mixes the crossing levels. Furthermore, we show that the difference observed in the relaxation rates also plays a crucial role in obtaining a consistent picture.

3. Maxwell–Schrödinger approach

This approach first implies the calculation of the macroscopic polarization $P(z, t)$, which is the (nuclear) medium's reaction to the electromagnetic field. The density matrix formalism is used to facilitate the statistical summations involved in obtaining $P(z, t)$ from the microscopic dipole moments. The polarization is then used to solve the (simplified) Maxwell equations in order to find the intensity of the transmitted radiation.

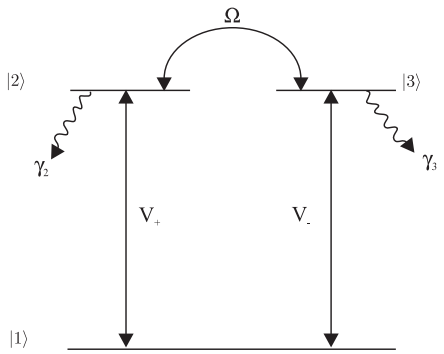

Figure 7. Schematic representation of the three-level system under consideration. The two excited states $|2\rangle$ and $|3\rangle$ are mixed by an interaction Ω and couple to the ground state through V_+ and V_-, respectively.

3.1. Three-level system in the parallel geometry

We start from the Liouville equation of motion for the density matrix operator $\hat{\rho}$ of the nuclear system:

$$\dot{\hat{\rho}} = -\frac{\mathrm{i}}{\hbar}[H, \hat{\rho}] - \widehat{\Gamma}\hat{\rho}, \tag{11}$$

with H the (Hermitian) Hamiltonian and $\widehat{\Gamma}$ a linear operator expressing all possible relaxations. We now apply this density matrix equations to the three levels involved in the level crossing/level mixing transition, i.e. the $|m_g = -1/2\rangle \equiv |1\rangle$ ground state and the $|m_e = 1/2\rangle \equiv |2\rangle$ and $|m_e = -3/2\rangle \equiv |3\rangle$ excited states. According to the selection rules for the parallel geometry, σ^+ polarized radiation (V_+) can induce a (2, 1) transition, whereas σ^- polarized radiation (V_-) induces a (3, 1) transition. We also include a mixing interaction (Ω) that allows for a (2, 3) transition. As argued before, this mixing interaction can have its origin in a non-axial component of the efg. The basic ingredients of this three-level system are summarized in figure 7.

In [25] the same three-level system is analyzed in a slightly different way. To allow an easy comparison, we follow the same line of reasoning and notation of that paper, wherever possible.

The Hamiltonian H of this system consists of an unperturbed part H_0 (which gives rise to the nuclear m states) and an interaction term:

$$H_1 = \hbar V_+ |2\rangle\langle 1| + \hbar V_- |3\rangle\langle 1| + \hbar\Omega |2\rangle\langle 3| + \text{h.c.} \tag{12}$$

The 14.4 keV gamma transition in ^{57}Fe is essentially an M1 magnetic dipole transition. Hence, the first two terms describe the interaction of the radiation with the nucleus in the magnetic dipole approximation, with $V_+ = \langle 2|\mathcal{H}^+|1\rangle\mathcal{E}^+(z,t)/2 \equiv \mu_c\mu_{21}\mathcal{E}^+(z,t)/2$ and $V_- = \langle 3|\mathcal{H}^-|1\rangle\mathcal{E}^-(z,t)/2 \equiv \mu_c\mu_{31}\mathcal{E}^-(z,t)/2$, with μ_c a proportionality constant. Explicit

expressions for the μ_{ij} matrix elements can be found in [26]. They are basically proportional to the product of a Wigner rotation matrix element and a Clebsch–Gordan coefficient. $\mathcal{E}^+(z,t)$ ($\mathcal{E}^-(z,t)$) is the space- and time-dependent part of the σ^+ (σ^-) polarized (electro)magnetic field.

The third term is a formal expression for the mixing interaction between the crossing levels, where the mixing frequency Ω is a measure of the strength of the mixing.

Applying equation (11) to this three-level system, the following set of density matrix equations is obtained:

$$\dot\rho_{11} = \gamma\rho_{22} + \gamma\rho_{33} - \mathrm{i}V_+(\rho_{21} - \rho_{12}) - \mathrm{i}V_-(\rho_{31} - \rho_{13}) \quad (13)$$

$$\dot\rho_{22} = -\gamma\rho_{22} - \mathrm{i}V_+(\rho_{12} - \rho_{21}) - \mathrm{i}\Omega(\rho_{32} - \rho_{23}) \quad (14)$$

$$\dot\rho_{33} = -\gamma\rho_{33} - \mathrm{i}V_-(\rho_{13} - \rho_{31}) - \mathrm{i}\Omega(\rho_{23} - \rho_{32}) \quad (15)$$

$$\dot\rho_{21} = \left(-\mathrm{i}\omega_0 - \frac{\gamma_2}{2}\right)\rho_{21} + \mathrm{i}V_+(\rho_{22} - \rho_{11}) - \mathrm{i}\Omega\rho_{31} + \mathrm{i}V_-\rho_{23} \quad (16)$$

$$\dot\rho_{31} = \left(-\mathrm{i}\omega_0 - \frac{\gamma_3}{2}\right)\rho_{31} + \mathrm{i}V_-(\rho_{33} - \rho_{11}) - \mathrm{i}\Omega\rho_{21} + \mathrm{i}V_+\rho_{32} \quad (17)$$

$$\dot\rho_{23} = -\frac{\gamma_2 + \gamma_3}{2}\rho_{23} - \mathrm{i}V_+\rho_{13} + \mathrm{i}V_-\rho_{21} + \mathrm{i}\Omega(\rho_{33} - \rho_{22}) \quad (18)$$

with $\omega_0 = \omega_2 - \omega_1$ ($\omega_2 = \omega_3$). The decay of the populations is related to γ, which corresponds to the natural decay rate of the nuclear excited state. The coherences, however, can have different decay rates due to other relaxation phenomena such as phase relaxation by the presence of a fluctuating magnetic hyperfine field [10, 26]. These decay rates are therefore given a different symbol, i.e. γ_2 and γ_3 (such that $\gamma_2, \gamma_3 \geqslant \gamma$).

We are interested in the solution of the ρ_{21} and ρ_{31} coherences since the polarizations of the medium are given by $P_+(z,t) = \mu_c\mu_{12}\rho_{21}$ and $P_-(z,t) = \mu_c\mu_{13}\rho_{31}$ [27]. The equations can be solved analytically in the linear response approximation. This means we consider the response of the medium only to first order in $V_\pm$. This is a good approximation since the interaction of the gamma radiation with the nuclei is small. In practice, it implies that we neglect the change of the populations ρ_{mm}. Instead, they are replaced with their initial values[3] $\rho^0_{11} = 1$ and $\rho^0_{22} = \rho^0_{33} = 0$. Also, since $\rho_{23} \propto V_\pm$ the $\mathrm{i}V_-\rho_{23}$ term in the equation for ρ_{21} and the $\mathrm{i}V_+\rho_{32}$ term in the equation for ρ_{31} are discarded.

The above set of equations is reduced to two coupled differential equations:

$$\dot\rho_{21} = \left(-\mathrm{i}\omega_0 - \frac{\gamma}{2}\right)\rho_{21} - \mathrm{i}V_+ - \mathrm{i}\Omega\rho_{31} \quad (19)$$

$$\dot\rho_{31} = \left(-\mathrm{i}\omega_0 - \frac{\gamma}{2}\right)\rho_{31} - \mathrm{i}V_- - \mathrm{i}\Omega\rho_{21} \quad (20)$$

where we have, for now, assumed that $\gamma_2 = \gamma_3 = \gamma$, which corresponds to the case when the normal lifetime decay is the only mechanism of relaxation. These differential equations can be simplified to algebraic equations by applying a Fourier transformation according to the recipe

$$F(\omega) = \int_{-\infty}^{\infty} \mathrm{d}t\, f(t)\mathrm{e}^{\mathrm{i}\omega t}, \quad (21)$$

[3] Actually, only half of the total initial population is in $|1\rangle$ since the other half occupies the $|m_g = 1/2\rangle$ state. As the three-level system is a closed system, we can renormalize the total initial population to the population in $|1\rangle$.

$$f(t) = \frac{1}{2\pi}\int_{-\infty}^{\infty} \mathrm{d}\omega\, F(\omega)\mathrm{e}^{-\mathrm{i}\omega t}. \quad (22)$$

The solution for the coherences in frequency domain is now given by

$$\rho_{21}(\omega) = \frac{L_+(\omega)}{2}V_+(\omega) + \frac{L_-(\omega)}{2}V_-(\omega), \quad (23)$$

$$\rho_{31}(\omega) = \frac{L_-(\omega)}{2}V_+(\omega) + \frac{L_+(\omega)}{2}V_-(\omega) \quad (24)$$

with

$$L_\pm = \frac{1}{\omega - \omega_0 - \Omega + \mathrm{i}\gamma/2} \pm \frac{1}{\omega - \omega_0 + \Omega + \mathrm{i}\gamma/2}. \quad (25)$$

The scattering amplitudes consist of a sum (or difference) of two Lorentzian lineshapes, which are centered around the frequencies of the mixed levels and are in anti-phase in the case of the polarization changing amplitudes.

The appropriate wave equations for an electromagnetic field in a reactive medium are given by the Maxwell equations, see, e.g., [28]. In most applications, however, a simplified version is used by assuming that the field functions slowly vary on the scale of the carrier wavelength λ_c. This is certainly a valid approximation in the case of gamma radiation. In the case of radiation propagating along the z axis (and thus neglecting variations of the field intensity in the transverse directions), the wave equations are reduced to [29]

$$\left(\frac{\partial}{\partial z} + \frac{n_h}{c}\frac{\partial}{\partial t}\right)\mathcal{E}_\pm(z,t) = \frac{2\pi\omega_c\rho_r}{n_h c}\mathrm{i}P^\pm(z,t), \quad (26)$$

with n_h the index of refraction of the host material, $\omega_c = c/\lambda_c$ the carrier frequency of the field and ρ_r the concentration of resonant nuclei. After Fourier-transforming these wave equations to frequency domain and substituting equations (23) and (24), we find

$$\left(\frac{\partial}{\partial z} - \mathrm{i}n_h k\omega\right)\begin{pmatrix}\mathcal{E}^+(z,\omega)\\ \mathcal{E}^-(z,\omega)\end{pmatrix} = \mathrm{i}\frac{2\pi k\rho_r}{n_h}\frac{\mu_c^2}{4} \times \begin{pmatrix}|\mu_{21}|^2L_+(\omega) & \mu_{21}\mu_{13}L_-(\omega)\\ \mu_{31}\mu_{12}L_-(\omega) & |\mu_{31}|^2L_+(\omega)\end{pmatrix}\begin{pmatrix}\mathcal{E}^+(z,\omega)\\ \mathcal{E}^-(z,\omega)\end{pmatrix}. \quad (27)$$

The solution for the electromagnetic field amplitudes is formally given by

$$\begin{pmatrix}\mathcal{E}^+(\omega,z)\\ \mathcal{E}^-(\omega,z)\end{pmatrix} = \mathrm{e}^{\mathrm{i}kz}\widetilde{S}(\omega,z)\begin{pmatrix}\mathcal{E}^+(\omega,0)\\ \mathcal{E}^-(\omega,0)\end{pmatrix} \quad (28)$$

with $\mathcal{E}^\pm(\omega,0)$ the field amplitudes of the incident radiation. The scattering matrix $\widetilde{S}(\omega,z)$ is calculated as

$$\widetilde{S}(\omega,z) = \frac{\mathrm{e}^{(a+d)/2}}{D} \times \begin{pmatrix}D\cosh\left(\frac{D}{2}\right) + (a-d)\sinh\left(\frac{D}{2}\right) & 2b\sinh\left(\frac{D}{2}\right)\\ 2c\sinh\left(\frac{D}{2}\right) & D\cosh\left(\frac{D}{2}\right) + (d-a)\sinh\left(\frac{D}{2}\right)\end{pmatrix} \quad (29)$$

with

$$a = \mathrm{i}\frac{2\pi}{k}\rho_r z f^{++}(\omega), \qquad b = \mathrm{i}\frac{2\pi}{k}\rho_r z f^{+-}(\omega),$$
$$c = \mathrm{i}\frac{2\pi}{k}\rho_r z f^{-+}(\omega), \qquad d = \mathrm{i}\frac{2\pi}{k}\rho_r z f^{--}(\omega), \quad (30)$$

$D = \sqrt{(a-d)^2 + 4bc}$ and the forward scattering amplitudes $f^{\sigma'\sigma}$:

$$f^{++}(\omega) = \frac{k^2\mu_c^2}{4n_h}|\mu_{21}|^2 L_+(\omega)$$
$$f^{--}(\omega) = \frac{k^2\mu_c^2}{4n_h}|\mu_{31}|^2 L_+(\omega) \quad (31)$$
$$f^{+-}(\omega) = \frac{k^2\mu_c^2}{4n_h}\mu_{21}\mu_{13} L_-(\omega)$$
$$f^{-+}(\omega) = \frac{k^2\mu_c^2}{4n_h}\mu_{31}\mu_{12} L_-(\omega). \quad (32)$$

Note that expression (29) exactly matches the expression for the scattering matrix obtained in [30, 31].

There is a one-to-one correspondence with the solution for the amplitude of the transmitted plane wave in the Blume–Kistner model [26] if we choose $n_h = 1$ and

$$\mu_c = \frac{1}{2\pi}\sqrt{\frac{VkT_e\gamma}{2\rho_r\hbar c\gamma_r}}, \quad (33)$$

where V is a quantization volume, γ the total decay rate and γ_r the radiative decay rate. In [25] it is shown that equation (27) can also be solved by finding two eigenmodes of $\mathcal{E}(\omega, z)$ which, after creation by a scattering on a first layer of resonant nuclei, propagate independently of one another through the medium. The results of that approach are exactly equal to those obtained in our analysis.

3.2. Thin absorber limit

To keep things analytical, we first consider the thin absorber limit ($T_e \ll 1$). Then, only the first terms in the Taylor expansion of the exponents in equation (29) are retained:

$$\begin{pmatrix}\mathcal{E}^+(\omega,z)\\ \mathcal{E}^-(\omega,z)\end{pmatrix} = e^{ikz}\left[\tilde{1} - i\frac{3T_e}{16}\frac{\gamma}{2}\begin{pmatrix}|C_{21}|^2 L_+(\omega) & C_{21}C_{13}L_-(\omega)\\ C_{31}C_{12}L_-(\omega) & |C_{31}|^2 L_+(\omega)\end{pmatrix}\right] \times \begin{pmatrix}\mathcal{E}^+(\omega,0)\\ \mathcal{E}^-(\omega,0)\end{pmatrix}, \quad (34)$$

with C_{ij} the product of the Clebsch–Gordan and rotation matrix coefficients of the $|j\rangle \rightarrow |i\rangle$ transition. The proportionality factor is obtained from the definition of the dipole matrix elements in [26]. We also use the definition of the effective thickness T_e (equation (1)) and the definition of the maximal resonant cross section σ_0 [22]:

$$\sigma_0 = \frac{2\pi}{k^2}\frac{2I_e+1}{2I_g+1}\frac{\gamma_r}{\gamma}. \quad (35)$$

Let us consider the case when σ^+ radiation is incident, $C_{12} = C_{13} = C_{12}^* = C_{13}^*$ and $C = 3T_eC_{12}^2/16$. For clarity, we omit the convolution with the incoming radiation. Then, the intensity of the transmitted radiation is given by

$$I(\omega) = |\mathcal{E}^+(\omega,z)|^2 + |\mathcal{E}^-(\omega,z)|^2 \quad (36)$$
$$= \underbrace{1 + 2\,\mathrm{Im}\left(C\frac{\gamma}{2}L_+(\omega)\right)}_{I_1(\omega)} + C^2\left|\frac{\gamma}{2}L_+(\omega)\right|^2 + C^2\left|\frac{\gamma}{2}L_-(\omega)\right|^2. \quad (37)$$

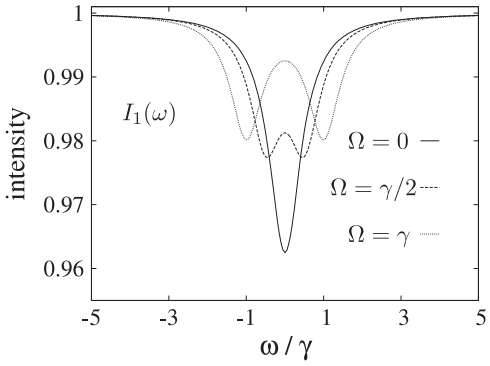

Figure 8. The transmitted radiation (up to first order in C) as a function of dimensionless frequency, for different values of the mixing interaction strength Ω (thin absorber limit $T_e = 0.1$).

In the thin absorber limit, $C \ll 1$ and, hence, the last two terms are negligible with respect to the first terms. The first term is the source term, which represents the case of transmission without scattering, while the second term represents the interference of the non-scattered with a single scattering event. The latter term can be rewritten as

$$2\,\mathrm{Im}\left(C\frac{\gamma}{2}L_+(\omega)\right) = -C\frac{\gamma^2}{2}\left(\frac{1}{(\omega-\omega_0-\Omega)^2+\frac{\gamma^2}{4}} + \frac{1}{(\omega-\omega_0+\Omega)^2+\frac{\gamma^2}{4}}\right), \quad (38)$$

which is a simple sum of two Lorentzian absorption lineshapes, centered at $\omega_0 \pm \Omega$, respectively. This means that there is only a (Stark) splitting of the levels, but no term that could describe additional interference effects.

As shown in figure 8, the absorption peaks of the first-order term are subtracted from the baseline (provided by the source term) giving rise to the well-known Mössbauer absorption spectrum. Note that this expression is equivalent to the absorption derived in [32], but which is now 'debunked' as two Lorentzian absorption lines.

3.3. Unequal relaxation rates

It is also possible to assume that the coherences involving the crossing levels have unequal relaxation rates ($\gamma_2 \neq \gamma_3$). A physical origin of such a difference may be found in the fluctuations of the magnetic hyperfine field, as mentioned previously. The transition with the highest Larmor frequency shows a higher relaxation rate, hence $\gamma < \gamma_2 < \gamma_3$, with γ the natural linewidth of the 14.4 keV nuclear excited state. The experimental data in section 2.4 strongly support this hypothesis. Figure 6 shows that $\gamma_3 \approx 2\gamma_2$.

We can solve equations (19) and (20) in exactly the same way as above, but now with $\gamma_2 \neq \gamma_3$:

$$\rho_{21}(\omega) = \frac{\delta_3}{\delta_+\delta_-}V_+(\omega) + \frac{\Omega}{\delta_+\delta_-}V_-(\omega) \quad (39)$$

$$\rho_{31}(\omega) = \frac{\Omega}{\delta_+\delta_-}V_+(\omega) + \frac{\delta_2}{\delta_+\delta_-}V_-(\omega), \quad (40)$$

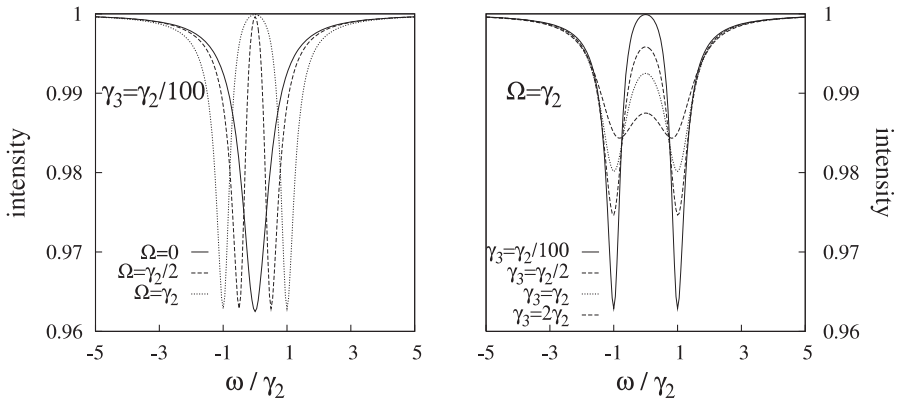

Figure 9. Simulation of the transmitted radiation in the case of: (left figure) the optical EIT regime ($\gamma_3 = \gamma_2/100$) for different values of Ω and (right figure) different values of γ_3 with a fixed mixing strength $\Omega = \gamma_2$ (thin absorber limit $T_e = 0.1$).

with

$$\delta_\pm = \omega - \omega_0 + i\frac{\gamma_2+\gamma_3}{4} \mp \sqrt{\Omega^2 - \left(\frac{\gamma_2-\gamma_3}{4}\right)^2} \tag{41}$$

$$\delta_{2/3} = \omega - \omega_0 + i\frac{\gamma_{2/3}}{2}. \tag{42}$$

Again, we limit our first analysis to the thin absorber case, following the same approach as before. Let us first consider the case when only σ^+ is incident. Because of the square root in the definition of $\delta_\pm$ we should distinguish two cases. Then, to first order in C (or T_e), the intensity of the transmitted radiation is given by

$$I'(\omega) = 1 + 2\,\mathrm{Im}\left(C\gamma\frac{\delta_3}{\delta_+\delta_-}\right) \tag{43}$$

$$= 1 - C\gamma\left[\frac{\gamma_2}{2}\left(g'_+(\omega)+g'_-(\omega)\right) + \left(\gamma_3\left(\Omega^2+\frac{\gamma_2\gamma_3}{4}\right) - \gamma_2\left(\frac{\gamma_2^2}{8}+\frac{\gamma_3^2}{8}-\Omega^2\right)\right)g'_+(\omega)g'_-(\omega)\right] \tag{44}$$

for $\Omega < |\gamma_2 - \gamma_3|/4$ and

$$I''(\omega) = 1 - C\gamma\left[\frac{\gamma_2}{2}\left(g''_+(\omega)+g''_-(\omega)\right) + (\gamma_3-\gamma_2)\left(\Omega^2+\frac{\gamma_2\gamma_3}{4}\right)g''_+(\omega)g''_-(\omega)\right] \tag{45}$$

for $\Omega \geqslant |\gamma_2 - \gamma_3|/4$, where we have introduced the notation

$$g'_\pm(\omega) = \frac{1}{(\omega-\omega_0)^2 + \left(\frac{\gamma_2+\gamma_3}{4} \mp \sqrt{\Omega^2 - \left(\frac{\gamma_2-\gamma_3}{4}\right)^2}\right)^2}, \tag{46}$$

$$g''_\pm(\omega) = \frac{1}{\left(\omega-\omega_0 \mp \sqrt{\Omega^2 - \left(\frac{\gamma_2-\gamma_3}{4}\right)^2}\right)^2 + \left(\frac{\gamma_2+\gamma_3}{4}\right)^2}. \tag{47}$$

It is seen that, as well as a Lorentzian contribution, there is the appearance of an interference term proportional to $g_+(\omega)g_-(\omega)$. When $\gamma_2 = \gamma_3$, the interference term vanishes and the transmitted radiation ($I''(\omega)$) reduces to the sum of Lorentzians, as obtained previously.

When $\gamma_3 \ll \gamma_2$, e.g. if $|3\rangle$ is a metastable state, the conditions for observing EIT are met[4]. Simulations of the intensity of the transmitted radiation for $\gamma_3 = \gamma_2/100$ are shown in the left part of figure 9. The effect of the interference term is quite dramatic. A *transparency window* is created where most absorption is canceled. At the center of the absorption line $I''(\omega=\omega_0)-1 \propto \gamma_3/(\Omega^2+\gamma_2\gamma_3/4)$, hence the absorption is completely suppressed only if $\gamma_3 = 0$. Also, in order to have a large reduction of the absorption, the condition that $\Omega^2 \gg \gamma_2\gamma_3/4$ should be fulfilled. These conclusions are in perfect agreement with the generic results of optical EIT, see, e.g., [33].

The importance of the value of γ_3 with respect to γ_2 is reflected in the spectra in the right-hand part of figure 9. It is clearly seen that, even in the presence of a mixing interaction (here $\Omega = \gamma_2$), there is no reduction but an *increase* in absorption at the line center if $\gamma_3 \geqslant \gamma_2$. This is also obvious from equation (45), where the sign of the interference term is determined by $(\gamma_3 - \gamma_2)$.

Let us now add the incidence of σ^- radiation. We only consider the most recurrent case of $\Omega \geqslant |\gamma_2-\gamma_3|/4$. Using the result in equation (45), the total transmitted radiation intensity is calculated as

$$I''(\omega) = 1 + 2\frac{3T_e}{16}\gamma\left[\mathrm{Im}\left(|C_{12}|^2\frac{\delta_3}{\delta_+\delta_-}\right) + \mathrm{Im}\left(|C_{13}|^2\frac{\delta_2}{\delta_+\delta_-}\right)\right]$$

$$= 1 - \frac{3T_e}{16}\gamma\left[\left(\frac{\gamma_2}{2}|C_{12}|^2 + \frac{\gamma_3}{2}|C_{13}|^2\right)\left(g''_+(\omega)+g''_-(\omega)\right) + \left(|C_{12}|^2 - |C_{13}|^2\right)(\gamma_3-\gamma_2) \times \left(\Omega^2+\frac{\gamma_2\gamma_3}{4}\right)g''_+(\omega)g''_-(\omega)\right]. \tag{48}$$

The addition of the σ^- contribution is of crucial importance for the interference term. Now, the sign of this term, which

[4] There are two other reasons why this special case corresponds to a 'common' optical EIT scheme. First, the restriction to the incidence of σ^+ radiation is equivalent to one probe field. Second, in the thin absorber limit, the possible transition $|3\rangle \to |1\rangle$, with emission of σ^- radiation, which is not present in a common EIT scheme, is neglected.

defines whether there is destructive (−) or constructive (+) interference, depends on the strength of one transition with respect to the other. For example, if $|C_{12}|^2 = |C_{13}|^2$, there is no observable interference, even if there is a mixing interaction *and* $\gamma_3 \ll \gamma_2$. This is, of course, due to the perfect symmetry of such a case, where the destructive and constructive terms exactly cancel each other. In our nuclear level mixing case, we have $|C_{12}|^2 = 1/3$, $|C_{13}|^2 = 1$ and $\gamma_3 \approx 2\gamma_2 \approx 2\gamma$, which yield a *net destructive interference* contribution. This is a promising result with regard to the explanation of the experimentally observed reduction of absorption.

Hence, we can conclude that a small but destructive interference term is present in the intensity of the transmitted gamma radiation at the level crossing. This is due to the combination of asymmetrical transition strengths and different relaxation rates, such that the strongest transition involves the level with the highest relaxation rate.

It is interesting to note that the integrated absorption over the full frequency range is *independent* of Ω. Although it seems that there is less absorption, which is of course true at the line center, this reduction is exactly compensated by an increase of absorption spread over the wings of the resonance. It would therefore be more appropriate to designate this effect as a *redistribution* instead of a reduction of absorption.

3.4. Three-level system in the perpendicular geometry.

In the perpendicular geometry, we must distinguish two different three-level systems. First, there is the $\Delta m = 0$ (or 2_a, see figure 1) transition from $|m_g = 1/2\rangle$ to the $|m_e = 1/2\rangle$ component of the mixed levels. The intensity of this absorption line is correctly described by equation (48) (or an extension of equation (44)) with $|C_{13}|^2 \approx 0$ because the $|-3/2\rangle \rightarrow |1/2\rangle$ is negligible with respect to the M1 transition. Then, it is clear that, for $\gamma_3 > \gamma_2$, the interference is always *constructive*, which gives rise to an enhanced absorption at the line center. Therefore, although there is a reduction of absorption due to splitting of the mixed levels, this reduction is partially counteracted by the interference term. This result explains why there is no important reduction observed at this absorption line (with respect to its partner line), while it is present in the parallel geometry.

The second three-level system involves the same states as in the parallel geometry. The difference now is that both polarization states of the incident radiation can induce both transitions (2, 1) and (3, 1) simultaneously. Taking into account the different relaxation rates, equations (39) and (40) are modified as

$$\rho_{21}(\omega) = \frac{\delta_3}{\delta_+\delta_-}\left(V_2^-(\omega) + V_2^-(\omega)\right) + \frac{\Omega}{\delta_+\delta_-}\left(V_3^+(\omega) + V_3^-(\omega)\right), \quad (49)$$

$$\rho_{31}(\omega) = \frac{\delta_2}{\delta_+\delta_-}\left(V_3^+(\omega) + V_3^-(\omega)\right) + \frac{\Omega}{\delta_+\delta_-}\left(V_2^+(\omega) + V_2^-(\omega)\right), \quad (50)$$

with $V_i^{\pm}(\omega) = \langle i|\mathcal{H}^{\pm}|1\rangle\mathcal{E}^{\pm}(z,\omega)/2 \equiv \mu_c\mu_{i1}^{\pm}\mathcal{E}^{\pm}(z,\omega)/2$. The polarizations of the medium are also changed accordingly: $P_{\pm}(z,t) = \mu_c\mu_{12}^{\pm}\rho_{21} + \mu_c\mu_{13}^{\pm}\rho_{31}$. These generalized expressions for the polarizations are substituted in the Fourier transformed propagation equation of equation (26). In the next section we discuss these equations through numerical simulations.

Table 1. Best fit values to the Maxwell–Schrödinger model of the $FeCO_3$ ($T_e = 8$) Mössbauer spectra for three different temperatures.

T	34 K		31 K		18 K	
θ	0	$\pi/2$	0	$\pi/2$	0	$\pi/2$
Γ_Ω (γ)	0.9	0.9	0.9(1)	0.9	0.9	0.9
β_e (mm s^{-1})	0.88(1)	0.87(1)	1.02(2)	1.02(2)	1.21(1)	1.21(1)
T_e	10(3)	9(1)	9(2)	10(3)	9(2)	9(4)
f_r	0.52(2)	0.55(5)	0.52(2)	0.57(4)	0.52(2)	0.54(6)
q_1	2.8(1)	3.2(1)	2.8(1)	3.0(1)	2.0(1)	1.9(2)
q_2	—	2.6(1)	—	2.5(1)	—	2.0(2)
q_3	1.6(1)	1.6(1)	1.5(1)	1.7(1)	2.0(1)	1.3(2)
$\chi^2_{r,\min}$	2.4	6.2	4.3	4.6	2.7	1.8
$\chi^2_{r,\min}$ (conv)	2.0	4.4	15.3	11.6	2.9	6.0

3.5. New fit

In order to fit the data in the case of a thick $FeCO_3$ crystal, the equations derived in the previous sections are solved numerically in the fitting program. The mixing interaction is taken into account in the following way. We assume that the magnitude of the non-axial component of the efg (labeled with Ω) is distributed in a Gaussian way around the mean value of $\overline{\Omega}$. This should be in much closer correspondence with the real conditions in the crystals than the assumption of a uniform non-zero value of Ω. In practice, we make a convolution of the initial spectrum $I(v, \Omega)$ with the Gaussian distribution $G(\Omega)$:

$$I(v, \overline{\Omega}) = \int_{-\infty}^{\infty} \mathrm{d}\Omega\, I(v, \Omega) G(\overline{\Omega} - \Omega), \quad (51)$$

with

$$G(\overline{\Omega} - \Omega) = \frac{1}{\Gamma_\Omega\sqrt{2\pi}} \mathrm{e}^{-\frac{1}{2}\left(\frac{\overline{\Omega}-\Omega}{\Gamma_\Omega}\right)^2} \quad (52)$$

and Γ_Ω the width of the distribution. In the fit, we choose $\overline{\Omega} = 0$, corresponding to the most prevalent situation in our $FeCO_3$ crystal and vary Γ_Ω.

The fitted results of the spectra of the $FeCO_3$ crystal at three different temperatures below T_N are summarized in table 1 and visualized in figures 10 and 11. First, we fit the spectrum in the parallel geometry at $T = 31$ K, yielding the reasonable value of $\Gamma_\Omega = 0.9(1)\gamma$. This value is kept fixed during the fitting of all other spectra (no estimated error). Also, to simplify the fitting procedure, the values of two hyperfine parameters are fixed to their mean value in the previous fits: IS = 1.33 m s^{-1} and $\Delta = 2.04$ mm s^{-1}. The three q_i values parameterize the line broadening. They are multiplied with the linewidth γ in the denominator of the forward scattering amplitudes $f^{\sigma'\sigma}(\omega)$ [34]. q_1 belongs to the $(3/2, 1/2) - (-3/2, -1/2)$ doublet, q_2 to the $(1/2, 1/2) - (-1/2, -1/2)$ doublet and q_3 to the $(1/2, -1/2) - (-1/2, 1/2)$ doublet.

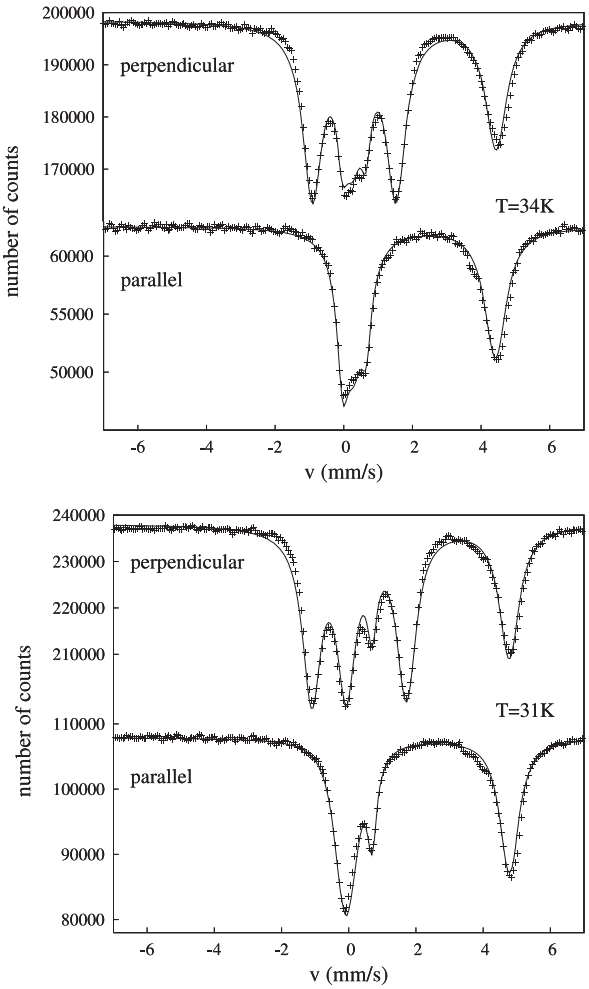

Figure 10. Mössbauer spectra of $T_e = 8$ at $T = 34$ and 31 K, with the solid line giving the best fit based on the Maxwell–Schrödinger model, taking into account different relaxation rates and a Gaussian-distributed Ω.

Not only do the fitted curves agree much better than before, although still with a slight misfit, with the experimental data, quantified in the reasonably small values of $\chi^2_{r,\min}$, but the derived values for the different parameters are also mutually consistent. For a better comparison with the previous fits, the last line in table 1 gives the previous values of χ^2, $\chi^2_{r,\min}$(conv). The transition-dependent broadening of the absorption lines (q_i values) is also in correspondence with the broadening deduced in the first Lorentzian analysis. Furthermore, the value obtained for T_e is close to its theoretical value of $T_e = 8$. The resonant fraction of the detected radiation, f_r, is a fitted parameter. It takes into account the recoilless fraction but also a correction for the non-resonant radiation due to the background coming from x-rays. The values obtained for f_r are, therefore, somewhat smaller than the critical value of the Mössbauer–Lamb factor $f_{LM} \approx 0.7$.

4. Conclusions

Mössbauer experiments have been performed using a $FeCO_3$ single crystal. A first analysis using Lorentzian absorption lines reveals a reduced absorption of gamma radiation at the level crossing in the parallel geometry. In the perpendicular geometry a similar transparency is observed. However, the 2_a transition, although it also involves the level crossing, does not show a reduced absorption. If the transparency mechanism was solely due to the Stark splitting of the mixed levels, as would be the case when they have equal relaxation rates, a reduction of absorption should be present in this 2_a transition.

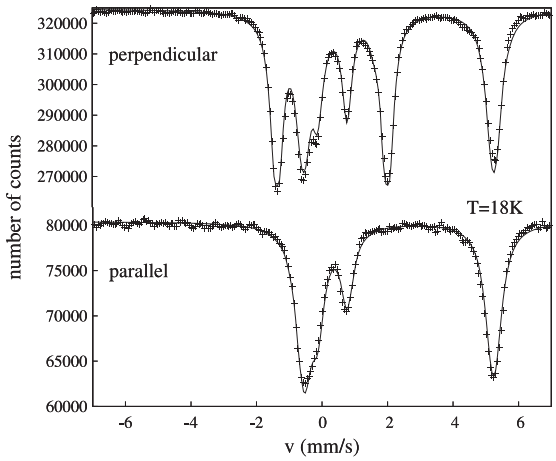

Figure 11. Mössbauer spectra of $T_e = 8$ at $T = 18$ K, with the solid line giving the best fit based on the Maxwell–Schrödinger model, taking into account different relaxation rates and a Gaussian distributed Ω.

From the experimental results, however, we learn that the transitions have unequal linewidths, originating from different relaxation rates due to a fluctuating magnetic field. We have shown that these unequal relaxation rates are crucial not only for the appearance of the interference term, but also for its sign. Now the *difference* between the three-level system in the parallel geometry and the '$\Delta m = 0$' three-level system in the perpendicular geometry is understood as a relaxation-dependent destructive and constructive interference term, respectively. Moreover, by implementing these new insights into a fitting program, we have finally succeeded in explaining the reduction of absorption in both geometries as *the combined effect of polarization, saturation and level-mixing-induced transparency in Λ schemes with different relaxation rates*.

Acknowledgments

This work was supported by FWO-Vlaanderen and the IAP P5/07 program of the Government of Belgium. SG is a research assistant of FWO-Vlaanderen.

References

[1] Coussement R *et al* 2002 *Phys. Rev. Lett.* **89** 107601
[2] Fleischhauer M, Imamoglu A and Marangos J P 2005 *Rev. Mod. Phys.* **77** 633

[3] Gheysen S, Coussement R, Muramatsu H, Shakhmuratov R N, Vyvey K and Odeurs J 2004 *J. Mod. Opt.* **51** 2589
[4] Gheysen S and Odeurs J 2006 *Phys. Rev.* B **74** 155443
[5] Alikhanov R A 1959 *Sov. Phys.—JETP* **36** 1204
[6] Jacobs I S 1963 *J. Appl. Phys.* **34** 1106
[7] Ono K and Ito A 1964 *J. Phys. Soc. Japan* **19** 899
[8] Housley R M, Gonser U and Grant R W 1968 *Phys. Rev. Lett.* **20** 1279
[9] Forester D W and Koon N C 1969 *J. Appl. Phys.* **40** 1316
[10] Ok H N 1969 *Phys. Rev.* **185** 472
[11] Boolchand P, Bresser W, Anaple G, Wu Y, Enzweiler R N, Coussement R and Grover J 1994 *Phys. Rev.* B **50** 6833
[12] Scoffin T P 1987 *An Introduction to Carbonate Sediments and Rocks* 1st edn (Glasgow: Blackie and Son)
[13] Klein C and Hurlbut C 1985 *Manual of Mineralogy* 20th edn (New York: Wiley)
[14] Cottenier S 2005 private communication
[15] Mössbauer R 1958 *Z. Phys.* **151** 124
[16] Waller I 1926 *Ann. Physik* **79** 261
[17] Lamb W E 1939 *Phys. Rev.* **55** 190
[18] Goldanskii V I, Makarov E F, Suzdalev I P and Vinogradov I A 1968 *Phys. Rev. Lett.* **20** 137
[19] Housley R M, Grant R W and Gonser U 1969 *Phys. Rev.* **178** 514
[20] Lagarec K 2002 *Recoil-Mössbauer Spectral Analysis Software for Windows* Mössbauer Group, University of Ottawa
[21] Brink D M and Satchler G R 1968 *Angular Momentum* (Oxford: Clarendon)
[22] Vértes A, Korecz L and Burger K 1979 *Mössbauer Spectroscopy* (Amsterdam: Elsevier)
[23] Blume M and Tjon J A 1968 *Phys. Rev.* **165** 446
[24] van der Woude F and Dekker A J 1965 *Solid State Commun.* **3** 319
[25] Shakhmuratov R N, Odeurs J, Gheysen S, Rostovtsev Y, Kocharovskaya O and Mandel P 2005 *Appl. Phys.* B **81** 883
[26] Blume M and Kistner O C 1968 *Phys. Rev.* **171** 417
[27] Scully M O and Zubairy S 1999 *Quantum Optics* (Cambridge: Cambridge University Press)
[28] Born M and Wolf E 1999 *Principles of Optics* 7th (expanded) edn (Cambridge: Cambridge University Press)
[29] Bloembergen N 1970 Review of nonlinear optical phenomena in condensed matter *Quantum Optics* (New York: Academic) pp 355–94
[30] Coussement R, Cottenier S and L'abbé C 1996 *Phys. Rev.* B **54** 16003
[31] Coussement R, Odeurs J, L'abbé C and Neyens G 2000 *Hyperfine Interact.* **125** 113
[32] Coussement R, Gheysen S, Serdons I, Callens R, Vyvey K, Shakhmuratov R N, Odeurs J, Mandel P, Rostovtsev Y and Kocharovskaya O 2003 *Hyperfine Interact.* **151** 93
[33] Mandel P 2001 *Hyperfine Interact.* **135** 223
[34] Smirnov G V 1996 *Hyperfine Interact.* **97/98** 551